

Submitted as a US Provisional Patent, Feb. 26, 2015, prepared Dec. 19, 2014 as an Invention Disclosure for the George Washington University.

**Title:**

**Carbon nanofibers, precious commodities from sunlight & CO<sub>2</sub> to ameliorate global warming**

Stuart Licht, Jiawen Ren

Department of Chemistry, George Washington University  
Washington, DC, 20052, USA.

This study introduces the high yield, electrolytic synthesis of carbon nanofibers, CNFs, directly from carbon dioxide. Production of a precious commodity such as CNFs from atmospheric carbon dioxide provides impetus to limit this greenhouse gas and mitigate the rate of climate change. CNFs are formed at high rate using inexpensive nickel and steel electrodes in molten electrolytes. The process is demonstrated as a scaled-up stand-alone electrolytic cell, and is also shown compatible with the STEP, solar thermal electrochemical process, using concentrated sunlight at high solar to electric efficiency to provide the heat and electrical energy to drive the CNF production.

Anthropogenic climate change consequences will be resolved when we inexpensively convert atmospheric carbon dioxide to diamonds yielding a compact, stable repository of CO<sub>2</sub> as valuable carbon. The global warming consequences of increasing atmospheric carbon dioxide concentrations are well established<sup>1,2</sup> as glacier and ice cap loss, sea level rise, droughts, hurricanes, species extinction, and economic loss. Here, we show another highly valued, stable, compact carbon, carbon nanofiber, CNF (not diamonds), that can be directly formed from atmospheric or exhaust CO<sub>2</sub> in an inexpensive process. Whereas the value per tonne of coal is ~\$60 and graphite is ~\$1,000, carbon nanofiber ranges from \$20,000 to \$100,000<sup>3</sup> per tonne. Today, CNFs require 30 to 100 fold higher production energy compared to aluminum<sup>4</sup>. The "production of CNTs and nano-fibers by electrolysis in molten lithium carbonate is impossible" according to the prior literature<sup>5</sup>. We present STEP (solar thermal electrochemical process) carbon nanofibers, in which solar energy efficiently drives the direct electrolytic conversion of CO<sub>2</sub>, dissolved in molten carbonates to CNFs at high rates using scalable, inexpensive nickel and steel electrodes. The structure is tuned by controlling the electrolysis conditions, such as the addition of trace nickel to act as CNF nucleation sites. We calculate that with an area <10% the size of the Sahara, the new STEP CNF can remove and decrease atmospheric CO<sub>2</sub> to pre-industrial revolution levels in ten years. New infrastructure and merchandise built from CNFs would provide a massive repository to store atmospheric CO<sub>2</sub>. CNFs are increasingly used in high strength, composite building materials ranging from top-end sports equipment to lightweight car and airplane bodies.<sup>3</sup> CNFs not only bind CO<sub>2</sub>, but will eliminate the massive CO<sub>2</sub> emissions associated with the production of steel, aluminum, and cement<sup>6-9</sup>, and will further decrease emissions by facilitating both wind turbines and lightweight, low carbon footprint transportation<sup>10</sup>.

Prior to the recognition of a variety of unique carbon nanoscopic structures such as fullerenes, nanotubes, and nanofibers starting in 1985<sup>11</sup>, the reduction of carbonates to (macroscopic) carbons in inorganic molten electrolytes from hydroxides and a barium chloride/ barium carbonate melt was recognized as early as the late 1800's<sup>12</sup>. Today, the principal methods of CNF preparation are (i) spinning of polymer nanofiber precursors followed by carbonization heat treatment<sup>13-15</sup> and (ii) catalytic thermal chemical vapor deposition (CVD) growth<sup>13,14</sup>. CVD growth of CNFs is catalyzed by metals or alloys, which are able to dissolve carbon to form metal carbides including nickel, iron, cobalt, chromium, and vanadium<sup>13,14,16</sup>. Low levels of the catalyst relative to CNF are required, and prominent catalyst nanoparticles are observed at the fiber tip, as well as catalyst clusters along the fiber that has migrated during CNF growth<sup>16</sup>. A variety of CNF morphologies have been observed including linear, coil, and sphere clustered CNFs<sup>13-18</sup>.

The electrochemical synthesis of CNFs has not been widely explored. Solid carbon electrodes have been electrolytically converted to nanostructures such as nanotubes in molten halide solutions via alkali metal formation, intercalation into, and exfoliation of the carbon<sup>19,20</sup>. Instead of the conversion of solid carbon, the rate of the direct reduction of CO<sub>2</sub> studied with carbon and platinum electrodes is limited by the low solubility of CO<sub>2</sub> in molten halides requiring high (15 atm) CO<sub>2</sub> pressure, and is accompanied by corrosion of the electrodes<sup>20,21</sup>. A study of 5-10% Li<sub>2</sub>CO<sub>3</sub> in molten chloride concluded that "production of CNTs and nano-fibers by electrolysis in molten lithium carbonate is impossible" because "Reduction and deposition of carbon occur instead of lithium discharge and intercalation into the cathode."<sup>5</sup> That is correct, but did not anticipate alternative CNF Ni nuclei growth paths from molten Li<sub>2</sub>CO<sub>3</sub> shown here.

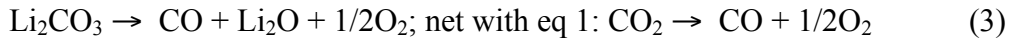
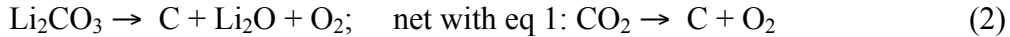
We have introduced STEP (the solar thermal electrochemical process), an alternative solar energy conversion process that uses the full spectrum of sunlight to drive solar syntheses of a range of energetic molecules at high solar efficiency. Solar thermal, high reactant concentrations, and unusual chemistries are used to decrease the energy required to drive endothermic electrolyses, and renewable electrical current is used to drive the low energy electrolysis<sup>22</sup>. STEP products are energetic molecules rather than electricity, and solar conversion efficiencies of 34 to 54% have been achieved<sup>6,23</sup>. STEP carbon<sup>6,23,24</sup>, STEP iron<sup>6-8,25</sup>, STEP organic<sup>26</sup>, STEP cement<sup>9</sup>, STEP Fuels<sup>27</sup>, and STEP ammonia<sup>28,29</sup> are among the processes which have been demonstrated. Here, we show the first demonstration in which STEP carbon is capable of generating pure carbon nanofibers from atmospheric carbon dioxide using molten carbonate electrolytes. Molten carbonates, such as pure Li<sub>2</sub>CO<sub>3</sub> (mp 723°C) or lower melting point carbonate eutectics such as LiNaKCO<sub>3</sub> (mp 399°C) or LiBaCaCO<sub>3</sub> (mp 620°C), mixed with highly soluble oxides, such Li<sub>2</sub>O and BaO, sustain rapid absorption of CO<sub>2</sub> from the atmospheric exhaust CO<sub>2</sub>. Equilibrium constraining lithium or lithium/barium oxide absorption has been presented, and the lithium case is described as<sup>6,8,24</sup>:



Air contains 0.04% CO<sub>2</sub>; this is only 1.7 x10<sup>-5</sup> mol of tetravalent carbon per liter, whereas molten carbonate contains ~20 mol of reducible tetravalent carbon per liter. A separate process to concentrate atmospheric CO<sub>2</sub> is not needed in STEP carbon. Hence, by absorbing CO<sub>2</sub> from the air, molten carbonates provide a million-fold concentration increase of reducible tetravalent carbon available for splitting (to carbon) in the

electrolysis chamber. Carbonate's higher concentration of active, reducible tetravalent carbon sites logarithmically decreases the electrolysis potential and can facilitate charge transfer at low electrolysis potentials. CO<sub>2</sub> is bubbled into the molten carbonate, and during electrolysis, oxygen is evolved at the anode while a thick solid carbon builds at the cathode (Figure 1). We observe that carbonate is readily split to carbon approaching 100% coulombic efficiency (coulombic efficiency is determined by comparing the moles of applied charge to the moles of product formed, where each mole of product formed depends on four moles of electrons) at molten carbonate temperatures of 750°C and below<sup>6,9,23,24</sup>; this is the case unless hydroxides are mixed with the carbonate, whereupon H<sub>2</sub> and carbon products are co-generated<sup>27</sup>. High current densities (>1 amp cm<sup>-2</sup>) of carbon formation<sup>5</sup> are sustained, and we observe similar sustained currents at carbon, platinum, or steel cathodes (the latter effectively become carbon electrodes during the deposition). Note via the Faraday equivalence that 1 A cm<sup>-2</sup> will remove 36 tonnes of carbon dioxide per m<sup>2</sup> cathode per year. Full cell electrolysis potentials range from ~1V under conditions of high temperature (*e.g.* 800°C), low current density (*e.g.* 10 mA cm<sup>-2</sup>), and high oxide concentration (*e.g.* 6 molal Li<sub>2</sub>O), to several volts. Conditions that increase carbonate electrolysis voltage are high current density, lower temperature, or lower oxide concentration.

At higher temperatures, the product gradually shifts to a mix of carbon and carbon monoxide, and it becomes pure CO by 950°C<sup>23</sup>. The respective 4- or 2-electron processes are given by:



Electrolysis, either via equation 2 or equation 3, releases Li<sub>2</sub>O to permit continued absorption of carbon dioxide (net: CO<sub>2</sub> is split and oxygen is released).

The SEM in Fig. 1 evidences no CNF in the carbon product deposited at the cathode subsequent to carbonate electrolysis in a nickel-free environment (Li<sub>2</sub>CO<sub>3</sub> at 730°C with 6 molal Li<sub>2</sub>O in the absence of nickel, utilizing a Pt rather than a Ni anode). Amorphous and platelet structures are seen, with the platelets indicative of partially formed multi-layered graphene/graphite. Electron dispersive spectroscopy elemental analysis indicates that the amorphous and platelet structures are composed of > 99% carbon. Similarly, CNF formation was not observed in the cathode product when the electrolysis was instead conducted with a Ni anode in a corrosion-free lower temperature (630°C) Li<sub>1.6</sub> Ba<sub>0.3</sub>Ca<sub>0.1</sub>CO<sub>3</sub> electrolyte.

We had not previously anticipated the oxygen generating anode effects on the structure of the carbon formed at the cathode during carbonate electrolysis. As demonstrated here, these anode effects are highly specific and can promote significant carbon nanofiber formation. We have investigated Pt, Ir, and Ni, and each can be effective as oxygen generating anodes<sup>6,8,23</sup>. Whereas Ir exhibits no corrosion following hundreds of hours use in molten carbonates, the extent of Ni corrosion is determined by the cation composition of the carbonate electrolyte. A nickel anode undergoes continuous corrosion in a sodium and potassium carbonate electrolyte<sup>27</sup>, it is stable after initial minor corrosion in lithium carbonate electrolytes<sup>8</sup>, and no corrosion of the nickel anode is evident in barium/lithium carbonate electrolytes<sup>24,27</sup>. In lithium carbonate electrolytes, we

have quantified the low rate of nickel corrosion at the anode as a function of anode current density, electrolysis time, temperature, and lithium oxide concentration<sup>9</sup>. The Ni loss at a 100 mA cm<sup>-2</sup> Ni anode in Li<sub>2</sub>CO<sub>3</sub> at 750°C with 0 or 5 molal added Li<sub>2</sub>O is respectively 0.5 or 4.1 mg cm<sup>-2</sup> of anode subsequent to 600 seconds of electrolysis, and increases to 4.6 or 5.0 mg cm<sup>-2</sup> subsequent to 1200 or 5400 seconds of electrolysis. The Ni loss increases to 7.0 mg or 13.8 mg cm<sup>-2</sup> respectively subject to higher current (1000 mA cm<sup>-2</sup>) or higher temperature (950°C). Each of these nickel losses tends to be negligible compared to the mass of Ni used in the various Ni wire or Ni shim configured anodes. Nickel oxide has a low solubility of 10<sup>-5</sup> moles NiO per mole of molten Li<sub>2</sub>CO<sub>3</sub><sup>30</sup>, equivalent to 10 mg Ni per kg Li<sub>2</sub>CO<sub>3</sub>. This low, limiting solubility constrains some of the corroded nickel to the anode surface as a thin oxide overlayer, with the remainder as soluble oxidized nickel available for reduction and redeposition at the cathode.

Electrolyte composition and current density substantially alter the nature of metal electrodeposition from molten carbonates. This is easy to observe with a more soluble metal salt, as opposed to one that is less soluble. We have recently demonstrated that iron (oxides), while insoluble in sodium or potassium carbonates, can become extremely soluble in lithiated molten carbonates, with solubility increasing with temperature to over 20% by mass Fe(III) or Fe(II) oxide<sup>6-8,25</sup>. The Extended Data Fig. 1 demonstrates that the size of deposited Fe varies inversely with current density from molten carbonates at a fixed charge (1Ah over a 10 cm<sup>2</sup> cathode), and that the iron shape is strongly affected by the electrolyte deposition conditions. Nickel oxide, unlike iron oxide, exhibits low solubility in lithium carbonate. However, as with nickel, we expect a wide variation of nickel deposition, with a variation of electrolysis conditions towards the goal of developing nickel as nucleation points to activate carbon nanofiber growth.

As will be demonstrated, even a low concentration of nickel originating from corrosion of the anode can deposit onto the cathode and catalyze carbon nanofiber formation. As illustrated in Fig. 2, higher nickel release during the carbonate electrolysis, which can be controlled due to the proportionality of the amount of nickel released by the size of the anode, results in a proliferation of CNFs of various diameters. As illustrated in Fig. 3, a lower concentration of controlled release of nickel results in the generation of highly homogeneous, smaller diameter CNFs. Both products were formed during electrolysis on a steel wire cathode in 730°C Li<sub>2</sub>CO<sub>3</sub> with added Li<sub>2</sub>O. The Fig. 2 carbon product was generated in a cell containing a purposefully oversized Ni anode, and the wide variety of carbon nanofibers generated in this single experiment range from ~0.2 to 4 μm in diameter and are up to 100μm in length.

As seen in the electron dispersive spectroscopy in Fig. 3, the bright spots are Ni deposits on the cathode. This is consistent with the known alternative CVD CNF growth mechanism, in which Ni acts as nucleation sites to initiate CNF growth<sup>16</sup>. The XRD diffraction peaks at 26° and 43° are assigned to the hexagonal graphite (002) and diffraction planes (JCPDS card files no. 41-1487) within the CNF (specifically, the stacking of parallel graphene layers and the size of graphene layer, respectively)<sup>10</sup>.

The predominant CNF cathode product is observed when the electrolysis is initiated at low current typically, 5 mA cm<sup>-2</sup>, followed by an extended high current electrolysis such as at 100 mA cm<sup>-2</sup>. The cathode product is principally amorphous (and only ~25% CNF), when staring directly at only a high (100 mA cm<sup>-2</sup>) current density. We interpret this mechanistically as follows: due to its low solubility, and lower reduction

potential, nickel (in this case originating from the anode) is preferentially deposited at low applied electrolysis currents (5 or 10 mA cm<sup>-2</sup>). This is evidenced by the low observed electrolysis voltage (<0.7V) and sustains the formation of nickel metal cathode deposits, which appear to be necessary to nucleate CNF formation. The concentration of electrolytic [CO<sub>3</sub><sup>2-</sup>] >> [Ni<sup>2+</sup>], and mass diffusion dictates that higher currents will be dominated by carbonate reduction. The subsequent higher electrolysis voltage thermodynamically required to deposit carbon<sup>23</sup> is only observed at higher applied currents (> 20 mA cm<sup>-2</sup>). Hence, without the initial application of low current, amorphous carbon will tend to form, while CNFs are readily formed following the low current nickel nucleation activation. In our typical high yield CNF electrolyses, the current is increased from 50 to 1000 mA at a 10 cm<sup>-2</sup> steel cathode over 15 minutes, followed by a constant current electrolysis at 1000 mA.

The CNF's synthesized in Fig. 3 utilized the same cathode and same composition electrolyte as in the Fig. 2 synthesis, but with a controlled, limited amount of nickel released to limit the Ni nucleation points forming on the cathode. This was accomplished by using a smaller (by one third) surface area of nickel anode in the electrolysis cell. The better resolved XRD peaks at 43° (100 plane) & 44° (101 plane) in Fig. 3 compared to Fig. 2 is evidence of better homogeneity of the CNFs synthesized under the Ni-limited conditions. As illustrated in Fig. 3, a lower concentration of controlled release of nickel results in the generation of highly homogeneous CNFs with a smaller, consistent diameter of ~0.2 μm.

The high nickel electrolysis product examined in the SEM of Fig. 2 present a proliferation of tangled carbon nanofibers of a wide variety of diameters. The low nickel electrolysis product examined in the SEM of Fig. 2 and 3 present a tangle of homogeneous-diameter carbon nanofibers. Each of those electrolyses utilized a molten Li<sub>2</sub>CO<sub>3</sub> electrolyte with 6 m added (dissolved) Li<sub>2</sub>O. Evidently, high concentrations of oxide localized in the nanofiber formation region leads to torsional effects (tangling). As shown in Fig. 4 carbon nanofibers grown by electrolysis in pure molten Li<sub>2</sub>CO<sub>3</sub> (without added Li<sub>2</sub>O) are consistently untangled, uniform and long. The nanofibers range from 300 to 1000 nm in width and 20 to 200 μm long.

The linear EDS map on the middle, right side of Fig. 4 shows elemental variation along the 6μm path of the EDS scan from pure Ni at the start of the fiber to pure C along the remainder of the fiber. Coulombic efficiency percent compares the moles of carbon recovered to applied each 4 moles of electrolysis charge in the reduction of CO<sub>2</sub>) and is over 80% (and approaches 100% with carefully recovery of all product after washing), the product (after washing off the electrolyte) consists of >80% pure carbon nanofibers. Initial results, indicative of whether the extent to which the nanofibers are hollow (tubes) or filled (threads), is seen in the SEM and TEM at the bottom of Fig. 4. Control of the number of carbon shells comprising the nanofiber, and the extent of filled fibers, and initial indications that Pt and Zn tend not to nucleate molten electrolytic CNF formation, but along with Ni, that Co, Cu and Mg might also induce CNF nucleation, will be presented in ongoing studies.

The CNF electrolysis chamber is readily scalable (Extended Data Fig. 2); we have scaled to 100A using 300 cm<sup>2</sup> (shown) and 800 cm<sup>2</sup> electrode cells, which scale the smaller cells both in lower carbon splitting potentials (1-1.5 V) and high (80-100 %) 4 electron coulombic efficiency of carbon product formation.

The demonstrated CNF synthesis can be driven by any electric source. As an alternative to conventionally generated electrical, we have also driven the CNF synthesis using electric current as generated by an illuminated efficient concentrator photovoltaic operating at maximum power point. We have previously heated CO<sub>2</sub> as a reactant for the electrolysis cell by (i) initially passing it over and under the concentrator photovoltaic (CPV), and then (ii) heating it to the electrolysis temperature using sub-band gap (infrared) thermal light split from concentrated sunlight (via a hot mirror) prior to absorption by the CPV.<sup>6</sup> In this study, to demonstrate the efficient solar synthesis of CNFs, we use an indoor solar simulator, and a 39% solar efficient CPV operating at 550 suns concentration (Extended Data Fig. 3), which has a maximum power point voltage of 2.7 V to drive two in-series (1.35V x 2) CNF electrolyzers at 2.3A. CNFs are efficiently formed from CO<sub>2</sub> in air, using inexpensive Ni and steel electrodes at high solar efficiency.

The demonstrated carbon dioxide to CNF process can consist of solar driven and solar thermal assisted CO<sub>2</sub> electrolysis. Large scale-up of STEP CNF could initiate with smokestack emissions providing a CO<sub>2</sub> reactant which is both hot and concentrated. An even greater amelioration of climate change will occur with the direct removal of atmospheric CO<sub>2</sub>. Extrapolating the present scale of the solar CNF synthesis determines that 700 km<sup>2</sup> of CPV in an area < 10% of that of the Sahara Desert will decrease atmospheric CO<sub>2</sub> to pre-industrial concentrations in ten years (Extended Data Schematic 1). Industrial environments provide opportunities to further enhance the CO<sub>2</sub> extraction rate; for example fossil-fuelled burner exhaust provides a source of relatively concentrated, hot CO<sub>2</sub> requiring less energy than the room temperature dilute CO<sub>2</sub> in the atmosphere. The product, carbon nanofiber may be stored as a stable, dense resource for future generations or stored in widespread use as a flexible, conductive, high strength material in carbon composites for infrastructure, transportation and consumer devices.

It is of interest whether material resources are sufficient to expand the process to substantially impact (decrease) atmospheric levels of carbon dioxide. The build-up of atmospheric CO<sub>2</sub> levels from a 280 to ~400 ppm occurring over the industrial revolution comprises an increase of 2 x 10<sup>16</sup> mole (8.2 x 10<sup>11</sup> metric tons) of CO<sub>2</sub>, and will take a comparable effort to remove. It would be preferable if this effort results in useable, rather than sequestered, resources. We calculate below a scaled up capture process can remove all excess atmospheric CO<sub>2</sub> converting it to useful carbon nanofibers.

Via the Faraday equivalence approaching 100% coulombic efficiency, 0.3 A cm<sup>-2</sup> will remove 10 tonnes of carbon dioxide per m<sup>2</sup> cathode per year, calculated as: 3x10<sup>3</sup> A m<sup>-2</sup> x 3.156x10<sup>7</sup> s year<sup>-1</sup> x (1 mol e<sup>-</sup> / 96485 As) x (CO<sub>2</sub>/ 4 e<sup>-</sup>) x (4.40098 x10<sup>-6</sup> tonne / mol) = 10 tonne CO<sub>2</sub>. At full absorption and conversion of CO<sub>2</sub>, this would require air with 0.04% CO<sub>2</sub> striking the cell with a wind speed of 1 mph per as: 1609 m air per h x 1 m<sup>2</sup> x 8,766 hour per year) x (0.0004 m<sup>3</sup> CO<sub>2</sub> / m<sup>3</sup> air) x 1 tonne per 556 m<sup>3</sup> CO<sub>2</sub> = 10 tonne CO<sub>2</sub>.

In STEP (solar thermal electrochemical process) CNF capture, 6 kWh m<sup>-2</sup> of sunlight per day, at 500 suns on 1 m<sup>2</sup> of 39% efficient CPV, will generate 430 kAh at 2.7 V to drive two series connected series connected molten carbonate electrolysis cells to form carbon nanofibers. As summarized in Extended Data Schematic 1, this will capture 8.1 x10<sup>3</sup> moles of CO<sub>2</sub> day<sup>-1</sup> to form solid carbon (based on 430 kAh · 2 series cells / 4 Faraday mol<sup>-1</sup> CO<sub>2</sub>). The material resources to decrease atmospheric carbon dioxide

concentrations with STEP CNF capture, appear to be reasonable. From the daily conversion rate of  $8.1 \times 10^3$  moles of  $\text{CO}_2$  per square meter of CPV, the capture process, scaled to  $700 \text{ km}^2$  of CPV operating for 10 years can remove and convert all the increase of  $2 \times 10^{16}$  mole of atmospheric  $\text{CO}_2$  to solid carbon. A larger current density at the electrolysis electrodes, will increase the required voltage and would increase the required area of CPVs. A variety of CSP installations, which include molten salt heat storage, are being commercialized, to permit 24/7, rather than daylight only, operation, and costs are decreasing. STEP provides higher solar energy conversion efficiencies than CSP, by producing a chemical product rather than electricity, and secondary losses can be lower (for example, there are no grid-related transmission losses). Contemporary concentrators, such as based on plastic Fresnel, rather than power towers have shorter focal length to avoid environmental thermal damage. Heat exchange losses are to be expected between hot,  $\text{CO}_2$ -cleansed air and ambient input air. A greater degree of solar concentration, for example 2000 suns, rather than 500 suns, will proportionally decrease the quantity of required CPV to  $175 \text{ km}^2$ , while the concentrator land area will be several thousand fold higher than the CPV area, equivalent to  $< 10\%$  of the area of the Sahara desert (which averages  $\sim 6 \text{ kWh m}^{-2}$  of daily sunlight over its  $10^7 \text{ km}^2$  surface), to remove anthropogenic carbon dioxide in ten years.

A related resource question is whether there is sufficient lithium carbonate, as an electrolyte of choice to decrease atmospheric levels of carbon dioxide for the STEP CNF carbon capture.  $700 \text{ km}^2$  of CPV plant will require several million tonnes of lithium carbonate electrolyte, depending on the electrolysis cell thickness current density and cell thickness. Thicker, or lower current density, cells will require proportionally more electrolyte. Fifty, rather than ten, years to return the atmosphere to pre-industrial carbon dioxide levels will require proportionally less electrolyte. These values are viable within the current production of lithium carbonate. Lithium carbonate availability as a global resource has been under scrutiny to meet the growing lithium battery market. It has been estimated that the annual production will increase to 0.24 million tonnes by 2015. Sodium and potassium carbonate are substantially more available and our study of these as alternate or mixed electrolytes is in progress.

Here, we show a highly valued, stable, compact carbon, carbon nanofiber, that can be directly formed from atmospheric or exhaust  $\text{CO}_2$  in an inexpensive process. Today, CNFs require 30 to 100 fold higher production energy compared to aluminum. We present the first high yield, inexpensive synthesis of carbon nanofibers from the direct electrolytic conversion of  $\text{CO}_2$ , dissolved in molten carbonates to CNFs at high rates using scalable, inexpensive nickel and steel electrodes. The structure is tuned by controlling the electrolysis conditions, such as the addition of trace nickel to act as CNF nucleation sites, limits to the electrolytic oxide concentration, and control of current density. New infrastructure and merchandise built from CNFs would provide a massive repository to store atmospheric  $\text{CO}_2$ .

## Methods

**Reagents.** Barium carbonate (Alfa Aesar, 99.5%), lithium carbonate (Alfa Aesar, 99%), lithium oxide (Alfa Aesar, 99.5%), and calcium carbonate (Alfa Aesar, 98%) are combined to form various molten electrolytes.

**Electrolyses.** Electrolyses are driven at a 2.3 A (amp) at the maximum power point of the illuminated concentrator photovoltaic as shown in Fig. 7, or galvanostatically at a set constant current (constant current) as described in the text. The electrolysis is contained in a pure alumina (AdValue, 99.6%) crucible or pure nickel crucible (Alfa Aesar). Alumina crucible electrolyses used coiled Ni wire (Alfa Aesar, 99.5%) as the (oxygen generating) anode or in scale-up experiments cylinders formed from pure Ni shim (McMaster 9707K5), while electrolyses in the Ni crucibles used the inner walls of the crucible as the anode. A wide variety of steel wires for coiled cathodes are effective, an economic form (used in this study) is Fi-Shock 14 Gauge, Steel Wire model #BWC-14200. During electrolysis, the carbon product accumulates at the cathode, which is subsequently removed and cooled. Details of solar (STEP methodology) electrolyses are provided in references 5, 6 and 28.

**Characterization.** The carbon product is washed, and analyzed by PHENOM Pro-X Energy Dispersive Spectroscopy on the PHENOM Pro-X SEM; by XRD analysis conducted at a sweep rate of 0.12 degree per minute on a Rigaku Miniflex diffractometer with a 0.01 degree slit width, analyzed using the Jade software package (JADE, 6:1; Materials Data, Inc. Livermore, CA, 2002); and by TEM, measured with a JOEL JEM-1200 EX Transmission Electron Microscope.

**Scale-up.** The STEP CNF electrolysis chamber is readily scalable; we have scaled to 100A using 300 (Extended data Fig. 2) and 800 cm<sup>2</sup> electrode cells driven with a Xantrex XTR 0-100 A DC power supply, which scale the smaller cells both in lower carbon splitting potentials (1-1.5 V) and high (80-100 %) 4 electron coulombic efficiency of carbon product formation. The larger cells use a cylindrical stainless steel 316 cylinder as a cathode sandwiched within concentric, cylindrical nickel anode anodes.

**Solar Electrolysis.** The process is demonstrated as a scaled-up stand-alone electrolytic cell, and is also shown to be with high solar to electric efficiency to drive the electrolytic CNF production. In the latter case, the electrolyzer current is provided by a 39% solar to electric efficient concentrator photovoltaic (0.3074 cm<sup>2</sup> Envoltek ESRD055 CPV) in lab under 1 kW Xenon, daylight color (5600K) AM1(air mass) illumination focused by Fresnel lens to to 550 suns concentration. As shown in Extended Data Fig. 3, the CPV is situated under the AM1 filter, with a fresnel concentrator above the AM 1 light source.



## Figure Legends

### Figure 1. CO<sub>2</sub> to carbon without carbon nanofibers in zero nickel environment.

Top middle, top right: typical maximum variation of observed cathodes subsequent to removal from carbonate electrolytes after a longer (4Ah) electrolysis in molten carbonate. Left photo shows 10cm<sup>2</sup> coiled steel wire (0.12 cm diameter) cathode prior to electrolysis. SEM of the washed cathode product subsequent to a nickel-free, 1.5 hour, 1 A constant current electrolysis in 730°C molten Li<sub>2</sub>CO<sub>3</sub> with 6 m Li<sub>2</sub>O using a 10cm<sup>2</sup> Pt foil anode and a 10cm<sup>2</sup> coiled steel wire (0.12 cm diameter) cathode, in a Ni-free crucible.

### Figure 2. CO<sub>2</sub> to a diverse range of carbon nanofibers from high nickel media

(subsequent to electrolysis with an oversized nickel anode, the inner wall of a 50 ml Ni crucible, at 0.05 A, then 1 A constant current electrolysis for 2 hours in 730°C molten Li<sub>2</sub>CO<sub>3</sub> with 6 m Li<sub>2</sub>O using a 10cm<sup>2</sup> coiled, 0.12 cm diameter steel wire). Top: X-ray powder diffraction of the carbon product. Middle, bottom: SEM of the washed cathode product subsequent to electrolysis with an oversized nickel cathode (the inner wall of a 50 ml Ni crucible). Consistent tangled fiber product with a wide range of diameter are observed throughout. Typical constant current electrolysis potentials range from 0.5 to 1.5 V as the current density is increased from 0.05 A to 1A.

### Figure 3. CO<sub>2</sub> to homogenous set of carbon nanofibers from controlled nickel media.

CO<sub>2</sub> to homogenous set of carbon nanofibers from controlled nickel media, 6 m added Li<sub>2</sub>O electrolyte. Left, middle: (repeated, representative of) EDS on fiber showing high carbon concentration; EDS Left, bottom: (repeated, representative) EDS on bright spot showing high nickel concentration. Right, bottom: SEM of washed cathode product subsequent to electrolysis with a smaller nickel cathode (the inner wall of a 20 ml Ni crucible), 0.05 A, then 1 A constant current electrolysis in 730°C molten Li<sub>2</sub>CO<sub>3</sub> with 6 m Li<sub>2</sub>O using a 10cm<sup>2</sup> coiled steel wire (0.12 cm diameter). Throughout the sample SEM consistently exhibited the same diameter CNFs. Top: X-ray powder diffraction of the cathode carbon product.

### Figure 4. CO<sub>2</sub> to homogenous, untangled set of carbon nanofibers from controlled nickel media, 0 added Li<sub>2</sub>O electrolyte.

SEM of the washed cathode product subsequent to electrolysis with a smaller nickel cathode (the inner wall of a 20 ml Ni crucible), 0.05 A, then 1 A constant current electrolysis in 730°C molten Li<sub>2</sub>CO<sub>3</sub> using a 10cm<sup>2</sup> coiled steel wire (0.12 cm diameter). Middle right: EDS composition mapping along the 6μ path, blue arrow path shown in the middle, left SEM. Lower right: TEM of fiber tip.

### Extended Data Figure 1. Fe variation with different electrolysis conditions.

Iron formed from 1.5 Ah of charge between a 10cm<sup>2</sup> Ni anode and a 10cm<sup>2</sup> iron cathode, at respective currents (from left to right and top to bottom) of 0.1A, 0.5 A, 2.5 A, 5A, 5A and 5A. In the first 5 panels the electrolysis was conducted in 730°C Li<sub>2</sub>CO<sub>3</sub> with 3 m Li<sub>2</sub>O and 1.5m Fe<sub>2</sub>O<sub>3</sub>, and in the last (lower right) panel 650°C Li<sub>1.6</sub>Ba<sub>0.3</sub>Ca<sub>0.1</sub>CO<sub>3</sub> with 6 m LiOH and 1.5m Fe<sub>2</sub>O<sub>3</sub>. Subsequent to water/dilute acid washing to remove excess electrolyte, EDS and titration<sup>28</sup> analysis distinguishes the amorphous particles as iron metal and the octahedra as Fe<sub>3</sub>O<sub>4</sub>. The presence of water available from the equilibrium

$2\text{LiOH} \rightleftharpoons \text{Li}_2\text{O} + \text{H}_2\text{O}$  in the latter electrolyte encourages the oxidation of deposited iron and formation of a product of octrahedral magnetite,  $\text{Fe}_3\text{O}_4$ .

**Extended Data Figure 2. Scaled-up electrolysis chamber splitting  $\text{CO}_2$  operating at 100 amp, 1.5V, and 95 to 100% coulombic efficiency of the 4 electron reduction to carbon.** Anode and cathode area  $300 \text{ cm}^2$ , alumina cell diameter 7 cm, height 14 cm. Top, left top: Concentric nickel anodes (electrically connected at bottom) with high current bus bar. Top, middle: steel cathode with high current bus prior to insertion between concentric anodes. Top, right: full cell prior to addition of the carbonate electrolyte. Bottom, left: Cathode subsequent to 1 hour, 100 A electrolysis at 1.5V with thick carbon deposited coating. Bottom, middle: Steel removal of carbon by striking cathode with hammer, and (view from bottom up) cathode with carbon layer removal nearly complete. Bottom, right: 2nd electrolysis with same electrodes yields same results.

**Extended Data Figure 3. Concentrator photovoltaic driving STEP CNF synthesis.** Electrolyzer current by power supply (initial experiments) and now provided by an efficient concentrator photovoltaic in lab under 1 kW Xenon, daylight color (5600K) AM1 (air mass) illumination. Left side is the  $0.3074 \text{ cm}^2$  Envoltek ESRD055 CPV situated under the air-cooled AM1 filter. Middle top: The Fresnel concentrator above the AM 1 filter. Middle bottom: the unattached CPC under the secondary optical concentrator. Right side: Typical (550 sun) photocurrent - voltage plot of the CPV.

**Extended Data Schematic 1. STEP carbon nanofiber to lower atmospheric  $\text{CO}_2$  to preindustrial levels in 10 years.** The required CPV and land area updated from 2010 STEP carbon and 2010  $\text{CO}_2$  concentration calculations in reference 23.

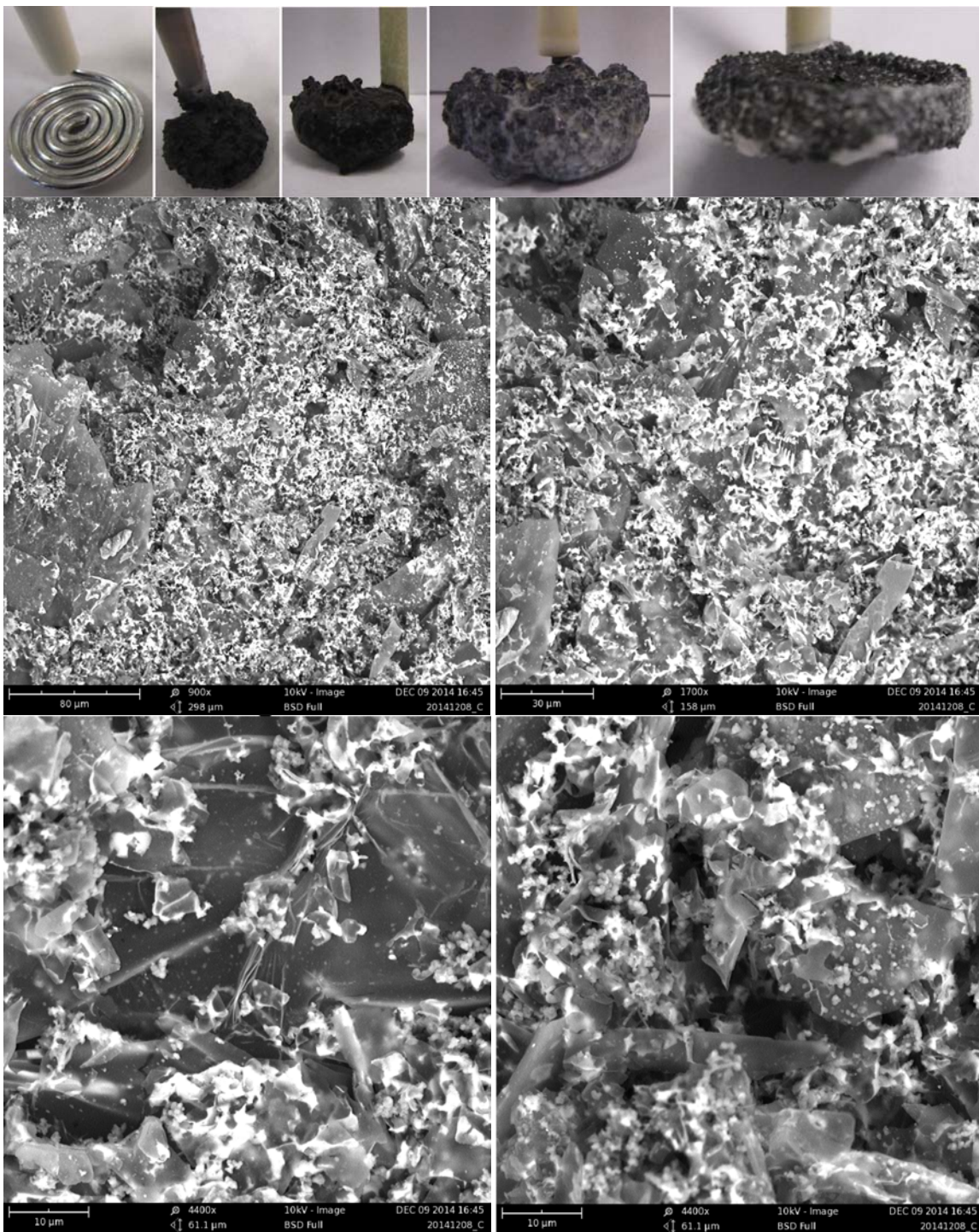


**Figure 1. CO<sub>2</sub> to carbon without carbon nanofibers in no nickel environment.**

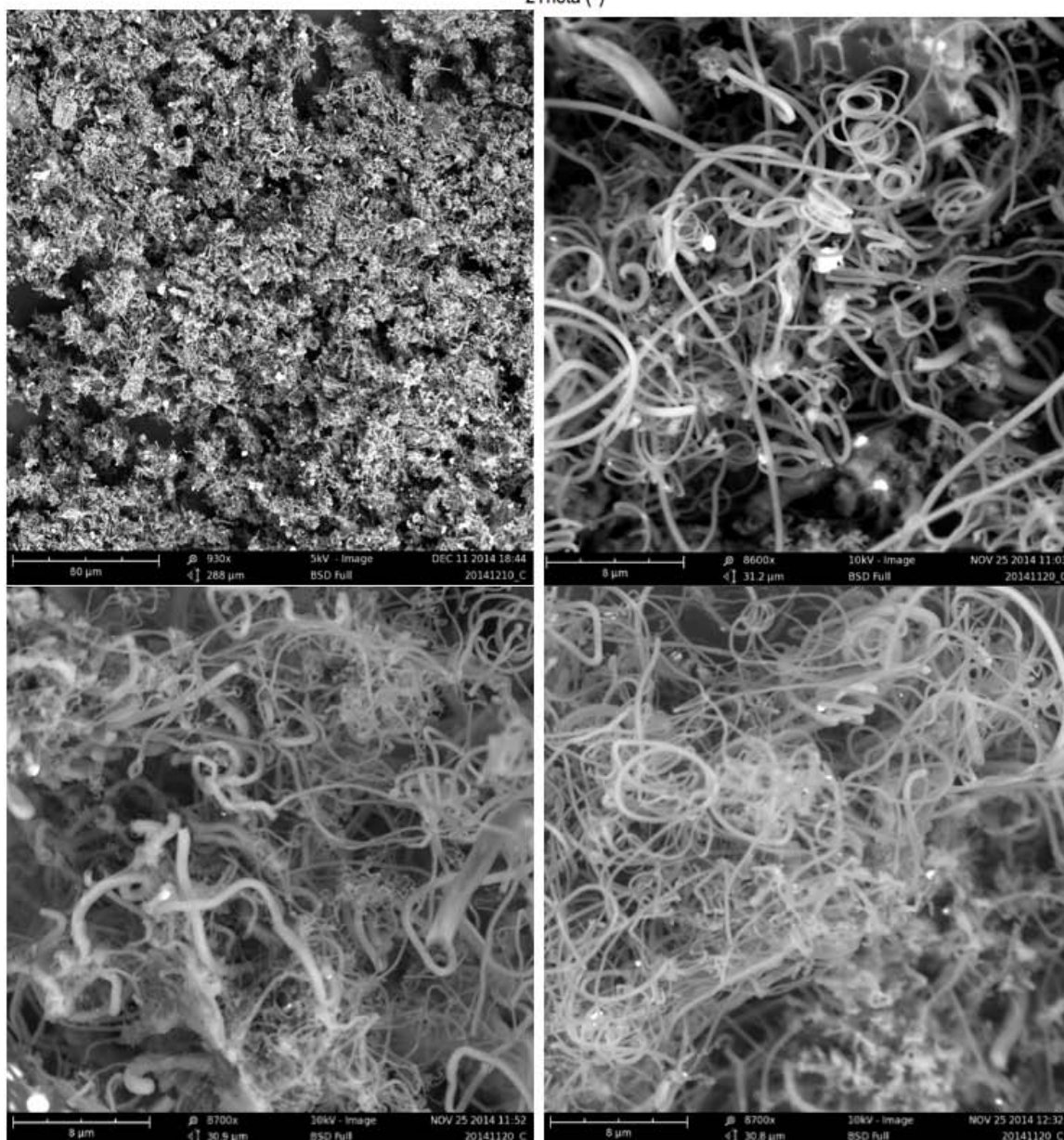
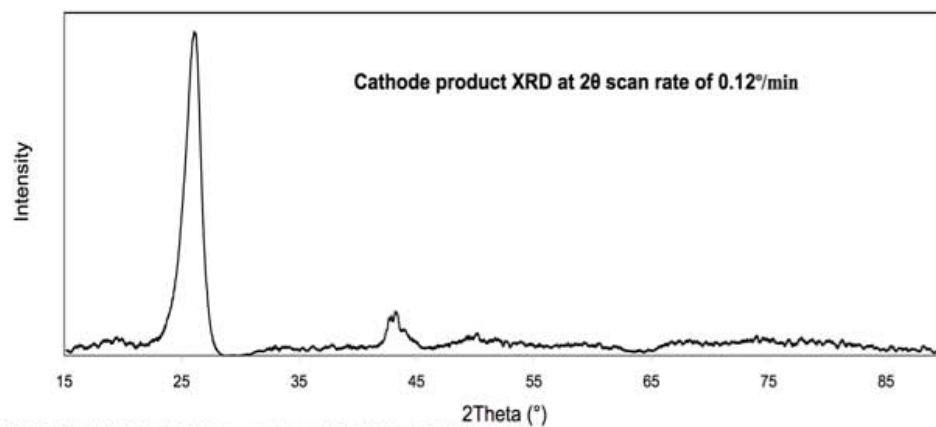
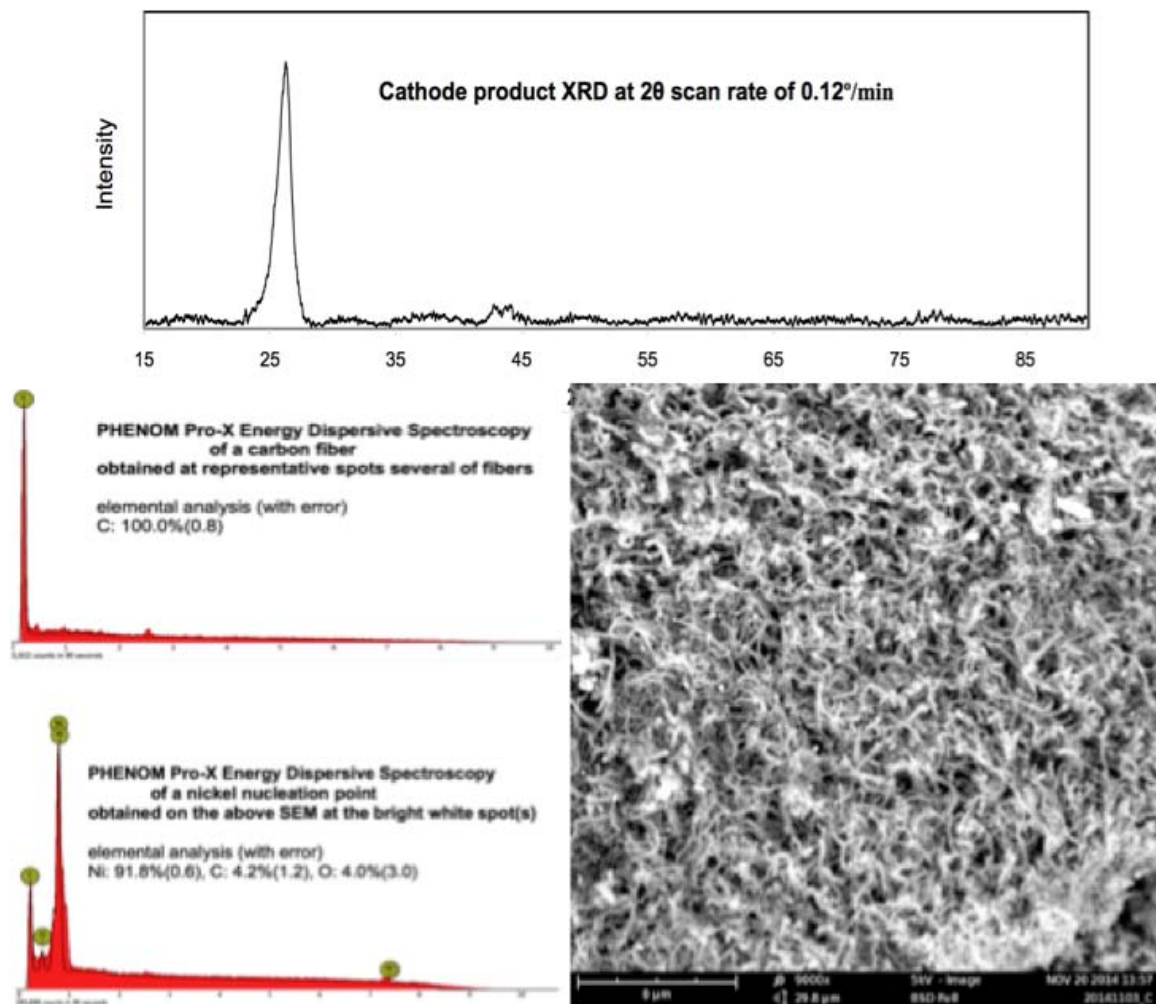
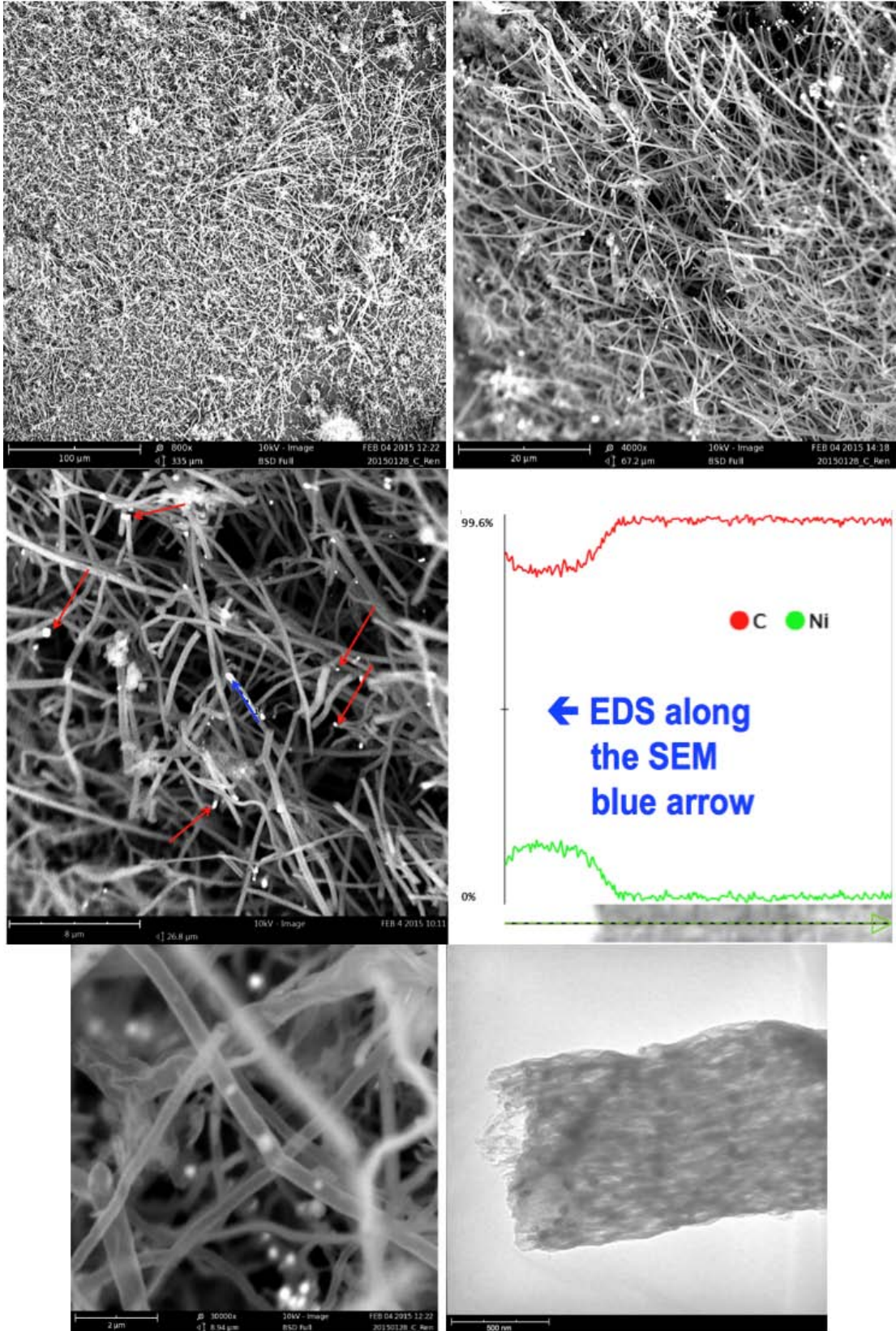


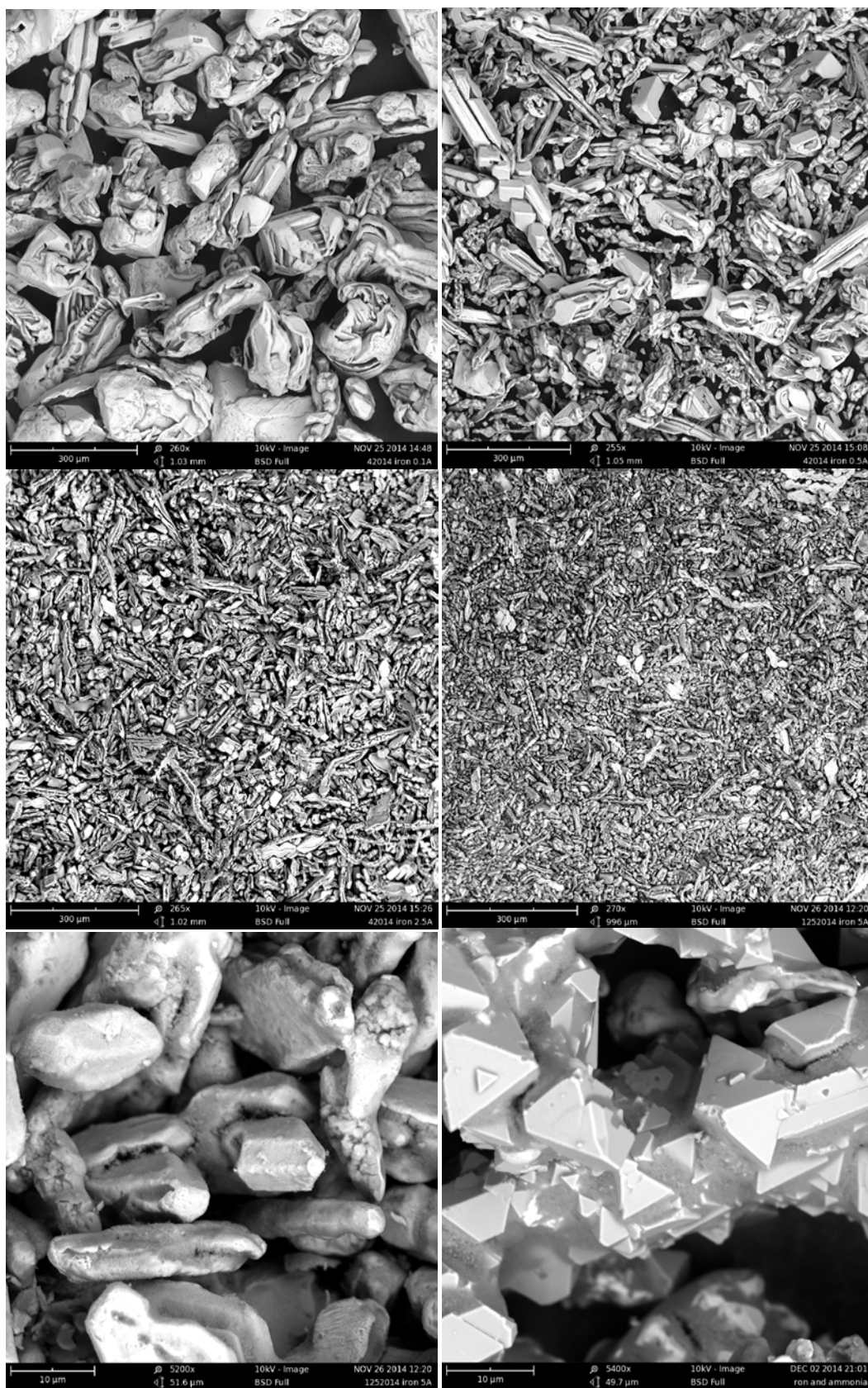
Figure 2. CO<sub>2</sub> to a diverse range of carbon nanofibers from high nickel media.



**Figure 3. CO<sub>2</sub> to homogenous set of carbon nanofibers from controlled nickel media.**



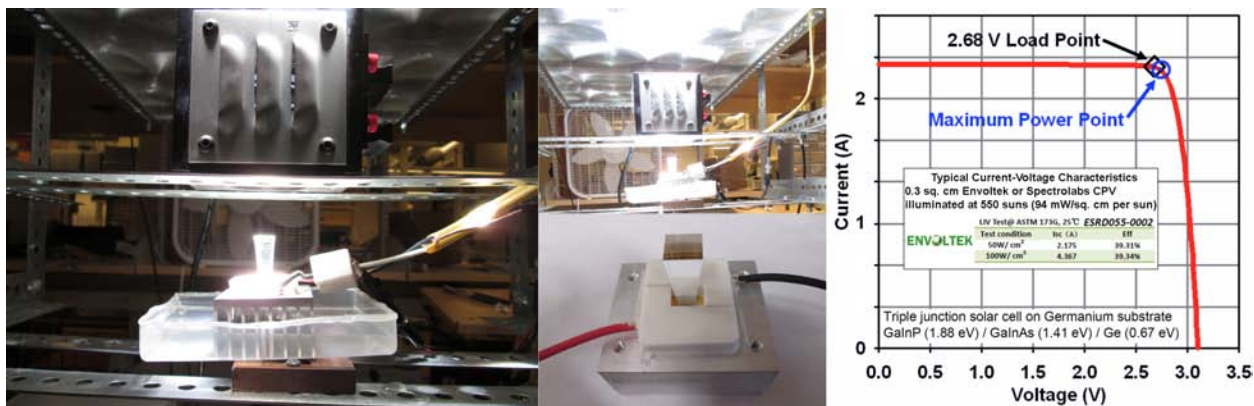
**Figure 4. CO<sub>2</sub> to homogenous, untangled set of carbon nanofibers from controlled nickel media, 0 added Li<sub>2</sub>O electrolyte.**



**Extended Data Figure 1. Fe variation with different electrolysis conditions.**



**Extended Data Figure 2. Scaled-up electrolysis chamber splitting CO<sub>2</sub> operating at 100 amp, 1.5V, and 95 to 100% coulombic efficiency of the 4 electron reduction to carbon.**



**Extended Data Figure 3. Concentrator photovoltaic driving STEP CNF synthesis.**



### Are resources sufficient to expand STEP CNF process to decrease atmospheric CO<sub>2</sub>?

◆ During the industrial revolution CO<sub>2</sub> has risen from 280 to 397 ppm, a **2x10<sup>16</sup> mole CO<sub>2</sub> increase**.

6 kWh m<sup>-2</sup> of sunlight **per day**, at 500 suns focused on 1 m<sup>2</sup> of 39% efficient CPV, will generate **430 kAh** at 2.7 V max power to drive **2 series** (1.35V each) connected molten carbonate electrolysis cells.

The demonstrated STEP solar efficiency of CO<sub>2</sub> conversion is > 39%, as it also incorporates waste CPV solar heat to heat the electrolysis. The challenge is to effectively direct this solar waste heat to CO<sub>2</sub> heating<sup>23</sup>: for example recovery from air heated rather than smoke-stack heated CO<sub>2</sub> converted to CNFs.

Daily, **430 kAh per day · 2 series electrolysis cells** / 4 Faraday mol<sup>-1</sup> CO<sub>2</sub>, will capture (per m<sup>2</sup> CPV): **8.1x10<sup>3</sup> moles of CO<sub>2</sub>** to form solid carbon nanofibers.

◆ From the daily conversion rate of **8.1 x10<sup>3</sup> moles of CO<sub>2</sub>** per day per square meter of CPV, scaled to 700 km<sup>2</sup> of CPV **STEP CNF operating for 10 years**: can convert/**decrease all the industry added atmospheric 2x10<sup>16</sup> mole of CO<sub>2</sub>** back to CNF.

Higher current density, will increase the electrolysis voltage and increase the required area of CPV, while higher solar concentration, will proportionally decrease the required CPV area.

◆ 700 km<sup>2</sup> of CPV will require a sunlight concentration area < < **10% of the 10<sup>7</sup> km<sup>2</sup> area of Sahara desert, for STEP CNF removal of anthropogenic carbon dioxide in 10 years.**

**Extended Data Schematic 1. STEP carbon nanofiber to lower atmospheric CO<sub>2</sub> to preindustrial levels in 10 years.**

## References

1. Bardgett, R. D. & Putten, W. H. Below biodiversity and ecosystem functioning. *Nature* **515**, 505–511 (2014)
2. Giosan, L., Syvitski, J., Constantinescu, & Day, J. Protect the world's deltas. *Nature* **516**, 31–33 (2014)
3. + composites, Part 4: Carbon fibre reinforced composites, at: <http://www.pluscomposites.eu/content/about-composites>  
pdf at:  
[http://www.pluscomposites.eu/sites/default/files/Technical%20series%20-%20Part%204%20-%20Carbon%20fibre%20reinforced%20composites\\_0.pdf](http://www.pluscomposites.eu/sites/default/files/Technical%20series%20-%20Part%204%20-%20Carbon%20fibre%20reinforced%20composites_0.pdf)  
site last modified Nov. 28, 2014
4. Kim, H. C., Fthenakis, V. Life cycle energy and climate change implications of nanotechnologies. *J. Industrial Ecology*, **17**, 528–541 (2012)
5. Dimitrov, A. T. Study of molten  $\text{Li}_2\text{CO}_3$  electrolysis as a method for production of carbon nanotubes. *Maced. J. Chem. Chem. Eng.* **28**, 111-118 (2009)
6. Licht, S. Efficient Solar-Driven Synthesis, Carbon Capture, and Desalination, STEP Production of Fuels, Metals, Bleach. *Advanced Materials*, **47**, 5592-5612 (2011)
7. Licht, S., Wang, B. STEP High Solubility Pathway for the Carbon Dioxide Free Production of Iron *Chem. Comm.* **47**, 7004-7006 (2010) ); *ibid*, **46**, 3081-3083 (2011)
8. Licht, S. Wu, H. STEP Iron, a Chemistry of Iron Formation without  $\text{CO}_2$  Emission: Molten Carbonate Solubility and Electrochemistry of Iron Ore Impurities. *J. Phys. Chem. C.*, **115**, 25138-25157 (2011)
9. Licht, S., Wu, H., Hettige, C., Wang, B., Lau, J., Asercion, J. Stuart, J. STEP Cement: Solar Thermal Electrochemical Production of  $\text{CaO}$  without  $\text{CO}_2$  emission *Chem. Comm.* **48**, 6019-6021 (2012)
10. Song, Y. S., Youn, J. R. & Gutowski, T. G. Life cycle energy analysis of fiber-reinforced composites. *Composites: Part A*, **40**, 1257–1265 (2009)
11. Iijima, S. Direct observation of the tetrahedral bonding in graphitized carbon black by high resolution electron microscopy. *J. Crystal Growth* **50**, 675-679 (1980)
12. Burkhardt, Z. *Chem.* **13**, 213 (1870); as referenced in. F. Haber and St. Tolloczko, Z. *Anorg. Chem.* F. Haber and St. Tolloczko, Z. *Anorg. Chem.* **10**, 407 (1904)
13. Feng, L., Xie, N. & Zhong, T. Carbon Nanofibers and Their Composites: A Review of Synthesizing, Properties and Applications. *Materials* **7**, 3919-3945 (2014)

14. Song, H., Wenzhong, S., Carbon Nanofibers: Synthesis and Applications. *J. Nanoscience Nanotech.* **14**, 1799-181 (2013)
15. Kurban, Z., Lovell, A., Jenkins, D., Bennington, S. Loader, II, Schober, A. & Skipper, N. Turbostratic graphite nanofibres from electrospun solutions of PAN in dimethylsulphoxide. *European Polymer Journal* **46**, 1194-1202 (2010)
16. Gao, J., Zhong, J., Bai, L., Liu J., Zhao, G. & Sun, X. Revealing the Role of Catalysts in Carbon Nanotubes and Nanofibers by Scanning Transmission X-ray Microscopy. *Scientific Reports* **4**, 1-6 (2014)
17. Liu, L., He, P., Zhou, K. & Chen, T. Microwave absorption properties of carbon fibers with carbon coils of different morphologies (double microcoils and single nanocoils) grown on them. *J Mater. Sci* **49**, 4379-4386 (2014)
18. Ko, S., Takahashi, Y., Sakoda, A., Sakai, Y. & Komori, K.. Direct Synthesis of Cup-Stacked Carbon Nanofiber Microspheres by the Catalytic Pyrolysis of Poly(ethylene glycol) *Langmuir* **528**, 8760-8766 (2012)
19. Hsu, W. K., Hare, J. P., Terrones, Kroto, H. W. & Walton, D. R. M. Condensed-phase nanotubes. *Nature* **377**, 687 (1995)
20. Dimitrov, A., Tomova, A., Grodzdanov A., Popovski, O. & Paunović, P. Electrochemical production, characterization, and application of MWCNTs. *J. Solid State Electrochem.* **17**, 399-407 (2013)
21. Novoselova, I. A., Oliynyk, Voronina, N. F. , Volkov, S. V., Konchits, A. A., Yanchuk, I. B., Yefanov, V. S., Kolesnik, S. P., Darpets, M. V. Electrolytic synthesis of carbon nanutubes from carbon dioxide in molten salts and their characterization. *Physica E* **40**, 2231-2237 (2008)
22. Licht, S. STEP (solar thermal electrochemical photo) generation of energetic molecules: A solar chemical process to end anthropogenic global warming. *J. Phys. Chem. C.*, **113**, 16283-16292 (2009)
23. Licht, S., Wang, B., Ghosh, Ayub, H., Jiang, D., Ganley, J. A New Solar Carbon Capture Process: STEP Carbon Capture, *J. Phys. Chem. Lett.* **1**, 2363-2368 (2010).
24. Licht, S., Cui, B., Wang, B. STEP Carbon Capture: the barium advantage. *J. CO<sub>2</sub> Utilization* Licht, S., 58-63 (2013)
25. Cui, B. Licht, S. Critical STEP advances for sustainable iron production. *Green Chem.* **15**, 881-884 (2013)
26. Zhu, Y., Wang, B., Liu, Z., Wang, H., Wu, H., Licht, S. STEP organic synthesis: an efficient solar, electrochemical process for synthesis of benzoic acid *Green Chem.* **16**, 4758-4766 (2014)

27. Li, F.-F., Liu, S., Cui, B., Lau, J., Stuart, J., Wang, B., Licht, S. A One-pot Synthesis of Hydrogen and Carbon Fuels from Water and Carbon Dioxide. *Advanced Energy Materials*, *in press* (2014)
28. Li, F.-F., Licht, S., Advances in understanding the mechanism and improved stability of the synthesis of ammonia from air and water in hydroxide suspensions of nanoscale Fe<sub>2</sub>O<sub>3</sub>. *Inorg. Chem.*, *53*, 10042-10044 (2014)
29. Licht, S., Cui, B., Wang, B. Li, F.-F., Lau, J., Liu, S. Ammonia synthesis by N<sub>2</sub> and steam electrolysis in molten hydroxide suspensions of nanoscale Fe<sub>2</sub>O<sub>3</sub>. *Science*, *345*, 637-640 (2014)
30. Ota, K., Mitshuima, S., Kato, S. Asano, S. Yoshitake, H. & Kaymiya, N. Solubilities of nickel oxide in molten carbonate. *J. Electrochem. Soc.* **139**, 667-671 (1992)